Based on the micro-CT analysis and the histological findings of this study, MSC-CM has dramatic effects on bone regeneration *in vivo*. Interestingly, bone regeneration following transplantation of hMSCs/agarose (MSCs group) was inferior to that following transplantation of MSC-CM. Further, our *in vitro* studies suggested that MSC-CM enhanced the migration and osteoinductivity of rMSCs. Based on these results, we hypothesized that MSC-CM stimulated the migration of endogenous rMSCs and accelerated new bone regeneration.

To confirm this hypothesis, and to visualize the dynamics of rMSCs *in vivo*, we imaged the movement of DiR-labeled rMSCs following injection into rats using an optical whole-body imaging technique. DiR was used to safely and directly label the membrane phospholipids of rMSCs. The proposed method of cellular staining is rapid (30-min incubation) and does not harm the cells. The rMSCs that were labeled with DiR were injected into the caudal vein of rats. The results of *in vivo* imaging suggested that rMSCs injected into the caudal vein migrated to the calvarial bone defect, where the MSC-CM was implanted. DiR fluorescence at the site at which MSC-CM was implanted continuously increased over time, suggesting that MSC-CM mobilized rMSCs to migrate to the implanted site. Although it is difficult to observe DiR-labeled cells in a deeper position by using the IVIS Imaging System, this method is useful for observing the behavior of cells close to, or on, bone surfaces, such as in calvarial bone. However, this analysis only mimicked endogenous mobilization of MSCs. To confirm that endogenous MSCs migrated to the site where the MSC-CM was implanted, we immunohistochemically stained cells in the bone defects of transgenic rats expressing GFP with anti-CD44 antibodies. CD44 is reported to be a specific marker of MSCs.[33] A number of CD44 and GFP double-positive cells were detected in the calvarial bone defects of the MSC-CM group of rats. On the other hand, there were fewer double-positive cells in the PBS group. In addition, tubular formations were seen in the regenerating bone of the MSC-CM group, suggesting the occurrence of angiogenesis in the calvarial bone defects of this group. This experiment indicated that MSC-CM has the potential to mobilize endogenous MSCs and to promote angiogenesis and bone regeneration.

Previous studies[23,34] of the factors present in MSC-CM using cytokine array analysis indicated that several cytokines and chemokines are present in MSC-CM and that these factors can influence several different types of cell behavior. In addition, MSC-CM also contains other factors that are present at a low level. We also found, using ELISA analysis, that IGF-1 and VEGF were present at high concentration in MSC-CM.

IGF-1 is known to be present in bone tissue and to be mitogenic for osteoblasts.[35] IGF-1 also increases the expression of CXCR4 and enhances SDF-1-induced MSCs migration through the PI-3-kinase (PI3K) pathway.[36]

VEGF is thought to be the main regulator of angiogenesis and bone marrow stromal cells secrete sufficient quantities of VEGF to enhance survival and differentiation of endothelial cells.[37] Further, IGF-1 induces VEGF mRNA in osteoblast-like cells through transcriptional mechanisms involving hypoxia-inducible factor-2α, and these events occur secondary to IGF-1 activation of the PI3K pathway during osteogenesis.[38,39] Based on this data, we hypothesized that bone regeneration induced by MSC-CM might be mediated by cooperative effects between IGF-1 and VEGF on angiogenesis and osteogenesis after endogenous cell mobilization.

Growth factors, such as BMP-2, have demonstrated great osteogenic potential[9,10] and are already on the market. However, unfortunately, application of these growth factors requires superphysiological doses[40] and may induce a severe inflammatory response.[11,41] Although Stephan *et al.* have demonstrated that BMP-2/chitosan gel can enhance bone regeneration in a rat calvarial model, an inflammatory response was also observed in histological findings.[42] Thus, although this growth factor can increase bone regeneration, it may also induce some severe complications. In addition, it has been considered that a combination of a number of factors can reduce the dose required and improve therapeutic effects. Some studies have investigated a mixture of two or more types of factors for bone regeneration.[13,14]

In this study, we used hMSCs and their cultured conditioned media for induction of bone regeneration because our aim was to apply MSC-CM to human patients. Several groups have recently shown that, although MSCs suppress T-lymphocyte proliferation, MSC-CM does not have a T-cell inhibitory effect *in vitro*.[43,44] Le Blanc *et al.* have reported that MSCs suppress T-cell proliferation that is induced by both allogeneic antigens and by mitogens, suggesting that this suppression is a nonspecific antiproliferative effect.[45] There is also evidence for *in vivo* immunosuppression by MSCs. Using a baboon skin graft model, Bartholomew *et al.* showed that MSCs appear to suppress alloreactivity *in vivo*.[46] On the other hand, the result of *in vivo* imaging and immunohistochemical staining of the present study suggest that MSC-CM implantation enhances the early mobilization of endogenous MSCs. Additionally, histological analysis suggested that strong inflammatory responses did not occur in the MSC-CM group. These findings can be explained by the fact that mobilized MSCs suppress T-lymphocyte proliferation, and therefore no obvious immune rejection reaction in the xenografts was observed throughout this study.

In addition, although our aim was bone regeneration, we did not use conditioned media derived from osteoblastic-differentiated hMSCs. Based on our obtained data, we hypothesize that the bone regeneration induced by MSC-CM might be mediated by cooperative effects between IGF-1 and VEGF on angiogenesis and osteogenesis after endogenous cell mobilization. Undifferentiated hMSCs rather than differentiated hMSCs have the potential for such cell behavior. We therefore consider that MSC-CM contains several cytokines and chemokines that regulate several different cell behaviors that are related to bone regeneration, which requires several steps, such as angiogenesis, cell migration, proliferation, and differentiation into osteoblasts. It should also be taken into consideration that not only IGF-1 and VEGF but also other factors that are present in MSC-CM at low concentration may contribute to bone regeneration and that the combination of these several factors can activate a variety of signaling pathways in order to regenerate bone. Further investigation will be necessary to explain how MSC-CM affects bone regeneration.

In this study, we showed that MSC-CM has very high potential for induction of bone regeneration without the necessity for stem cell transplantation. This is the first report of the use of stem-cell-cultured conditioned media for

induction of bone regeneration *in vitro* and *in vivo*. This novel regenerative medicine is based on a unique concept that utilizes endogenous stem cells without stem cell transplantation. This regenerative medicine approach will also reduce several of the problems that are currently encountered in clinical applications of stem cells, such as problems of expense, time, and safety.

Acknowledgments

The authors wish to thank Drs. Akihito Yamamoto, Kazuhiko Kinoshita, Minoru Inoue, Ms. Mami Naruse, and the members of the Department of Oral and Maxillofacial Surgery as well as Mr. Shinsuke Kimura of Hitachi Aloca Medical, Ltd., for their help and contributions to the completion of this study. This work was supported in part by Grants-in-Aid for Scientific Research (Nos. 21791985 and 23592883) from the Ministry of Education, Culture, Sports, Science, and Technology of Japan.

Disclosure Statement

No competing financial interests exist.

References

1. Barome, A., and Covani, U. Maxilary alveolar ridge reconstruction with nonvasculized autogenous block bone: clinical results. J Oral Maxillofac Surg **65,** 2039, 2007.
2. Kurz, L.T., and Grafin, S.R., and Booth, R.E. Harvesting autogenous iliac bone grafts. A review of complications and techniques. Spine **14,** 1324, 1989.
3. Athanasiou, V.T., Papachristou, D.J., Panagopoulos, A., Saridis, A., Scopa, C.D., and Megas, P. Histological comparison of autograft, allograft-DBM, xenograft, and synthetic grafts in a trabecular bone defect: an experimental study in rabbits. Med Sci Monit **16,** BR24, 2010.
4. Eppley, B.L., Pietzak, W.S., and Blanton, M.W. Allograft and alloplastic bone substitutes: a review of science and thchnology for the craniomaxillofacial surgeon. J Craniofac Surg **16,** 981, 2005.
5. Moore, W., Graves, S.E., and Bain, G.I. Synthetic bone graft substitutes. ANZ J Surg **71,** 354, 2001.
6. Kaigler, D., Cirelli, J.A., and Giannobile, W.V. Growth factor delivery for oral and periodontal tissue engineering. Expert Opin Drug Deliv **3,** 647, 2006.
7. Sykaras, N., and Opperman, L.A. Bone morphogenetic proteins (BMPs): how do they function and what can they offer the clinician? J Oral Sci **45,** 57, 2003.
8. Linkhart, T.A., Mohan, S., and Baylink, D.J. Growth factors for bone regeneration and repair: IGF, TGFβ and BMP. Bone **19,** 1S, 1996.
9. Shimazu, S., Hara, T., Kinuta, Y., Moriya, K., Maruo, Y., Hanada, S., and Minagi, S. Enhanced vertical alveolar bone augmentation by recombinant human bone morphogenic protein-2 with carrier in rats. J Oral Rehabil **33,** 609, 2006.
10. Herford, A.S., and Boyne, P.J. Reconstruction of mandibular continuity defects with bone morphogenic protein-2 (rhBMP-2). J Oral Maxillofac Surg **66,** 616, 2008.
11. Perri, B., Cooper, M., Lauryssen, C., and Anand, N. Adverse swelling associated with use of rh-BMP-2 in anterior cervical discectomy and fusion: a case study. Spine J **7,** 235, 2007.
12. Vaidya, R., Carp, J., Sethi, A., Bartol, S., Craig, J., and Les, C.M. Complications of anterior cervical discectomy and fusion using recombinant human bone morphogenetic protein-2. Eur Spine J **16,** 1257, 2007.
13. Chen, L., Jiang, W., Huang, J., He, B., Zuo, G., Zhang, W., Luo, Q., Shi, Q., Zhang, B., Wagner, E.R., Luo, J., Tang, M., Wietholt, C., Luo, X., Bi, Y., Su, Y., Liu, B., Kim, S.H., He, C.J., Hu, Y., Shen, J., Rasteger, F., Huang, H., Gao, Y., Gao, J., Zhou, J., Reid, R.R., Luu, H.H., Haydon, R.C., He, T., and Deng, Z. Insulin-like growth factor 2 (IGF-2) potentiates BMP-9-induced osteogenic differentiation and bone formation. J Bone Miner Res **25,** 2447, 2010.
14. Ozaki, Y., Nishimura, M., Sekiya, K., Suehiro, F., Kanawa, M., Nikawa, H., Hamada, T., and Kato, Y. Comprehensive analysis of chemotactic factors for bone marrow mesenchymal stem cells. Stem Cells Dev **16,** 119, 2007.
15. Langer, R., and Vacanti, J.P. Tissue engineering. Science **260,** 920, 1993.
16. Menasché, P., Alfieri, O., Janssens, S., McKenna, W., Reichenspurner, H., Trinquart, L., Vilquin, J.T., Marolleau, J.P., Seymour, B., Larghero, J., Lake, S., Chatellier, G., Solomon, S., Desnos, M., and Hagège, A.A. The myoblast autologous grafting in ischemic cardiomyopathy (MAGIC) trial: first randomized placebo-controlloed study of myoblast transplantation. Circulation **117,** 1189, 2008.
17. Morigi, M., Introna, M., Imberti, B., Corna, D., Abbate, M., Rota, C., Rottoli, D., Benigni, A., Perico, N., Zoja, C., Rambaldi, A., Remuzzi, A., and Remuzzi, G. Human bone marrow mesenchymal stem cells accelerate recovery of acute renal injury and prolong survival in mice. Stem Cells **26,** 2075, 2008.
18. Colter, D.C., Class, R., DiGirolamo, C.M., and Prockop, D.J. Rapid expansion of recycling stem cells in cultures of plastic-adherent cells from human bone marrow. Proc Natl Acad Sci U S A **97,** 3213, 2000.
19. Jiang, Y., Jahagirdar, B.N., Reinhardt, R.L., Schwartz, R.E., Keene, C.D., Oritz-Gonzalez, X.R., Reyes, M., Lenvik, T., Lund, T., Blackstad, M., Du, J., Aldrich, S., Lisberg, A., Low, W.C., Largaespada, D.A., and Verfaillie, C.M. Pluripotency of mesenchymal stem cells derived from adult marrow. Nature **418,** 41, 2002.
20. Yamada, Y., Ueda, M., Naiki, T., Takahashi, M., Hata, K., and Nagasaka, T. Autogenous injectable bone for regeneration with mesenchymal stem cells (MSCs) and platelet-rich plasma (PRP)–tissue-engineered bone regeneration. Tissue Eng **10,** 955, 2004.
21. Yamada, Y., Nakamura, S., Ito, K., Kohgo, T., Hibi, H., Nagasaka, T., and Ueda, M. Injectable tissue-engineered bone using autogenous bone marrow-derived storomal cells for maxillary sinus augmentation: clinical application ewport from 2-6-year follow-up. Tissue Eng Part A **14,** 1699, 2008.
22. Ide, C., Nakai, Y., Nakano, N., Seo, T., Yamada, Y., Endo, K., Noda, T., Saito, F., Suzuki, Y., Fukushima, M., and Nakatani, T. Bone marrow stromal cell transplantation for treatment of sub-acute spinal cord injury in rat. Brain Res **1332,** 32, 2010.
23. Chen, L., Tredget, E.E., Wu, P.Y.G., and Wu, Y. Paracrine factors of mesenchymal stem cells recruit macrophages and endothelial lineage cells and enhance wound healing. PLoS One **3,** e1886, 2008.
24. Ponte, L.A., Maris, E., Gallay, N., Langonne, A., Delorme, B., Herault, O., Charbord, P., and Domenech, J. The *in vitro* migration capacity of human bone marrow mesenchymal stem cells: comparison of chemokine and growth factor chemotactic activities. Stem Cells **25,** 1737, 2007.

25. Kinnaird, T., Srabile, E., Burnett, M.S., Shou, M., Lee, C.W., Barr, S., Fuchs, S., and Epstein, S.E. Local delivery of marrow-derived stromal cells augments collateral perfusion through paracrine mechanisms. Circulation **109,** 1543, 2004.
26. Azizi, S.A., Stokes, D., Augelli, B.J., DiGirolamo, C., and Prockop, D.J. Engraftment and migration of human bone stromal cells implanted in the brains of albino rats–similarities to astrocyte grafts. Proc Natl Acad Sci U S A **95,** 3908, 1998.
27. Wislet-Gendebien, S., Leprince, P., Moonen, G., and Rogister, B. Regulation of neural markers nestin and GFAP expression by cultivated bone marrow stromal cells. J Cell Sci **116,** 3295, 2003.
28. Gibson, U.E., Heid, C.A., and Williams, P.M. A novel method for real time quantitative RT-PCR. Genome Res **6,** 995, 1996.
29. Heid, C.A., Stevens, J., and Williams, P.M. Real time quantitative PCR. Genome Res **6,** 986, 1996.
30. Kalchenko, V., Shivtiel, S., Malina, V., Lapid, K., Haramati, S., Lapidot, T., Brill, A., and Harmelin A. Use of lipophilic near-infrared dye in whole-body optical imaging of hematopoietic cell homing. J Biomed Opt **11,** 50507, 2006.
31. Ito, T., Suzuki, A., Imai, E., Okabe, M., and Hori, M. Bone marrow is a reservoir of repopulating mesangial cells during glomerular remodeling. J Am Soc Nephrol **12,** 2625, 2001.
32. Kawamoto, T. Use of a new adhesive film for the preparation of multi-purpose fresh-frozen sections from hard tissues, whole-animals, insects and plants. Arch Histol Cytol **66,** 123, 2003.
33. Sonoda, E., Aoki, S., Uchihashi, K., Soejima, H., Kanaji, S., Izuhara, K., Satoh, S., Fujitani, N., Sugihara, H., and Toda, S. A new organotypic culture of adopose tissue fragments maintains viable mature adipocytes for a long term, together with development of immature adipocytes and mesenchymal stem cell-like cells. Endocrinology **149,** 4794, 2008.
34. Nakano, N., Nakai, Y., Seo, T.B., Yamada, Y., Ohno, T., Yamanaka, A., Nagai, Y., Fukushima, M., Suzuki, Y., Nakatani, T., and Ide, C. Characterization of conditioned medium of cultured bone marrow stromal cells. Neurosci Lett **483,** 57, 2010.
35. Spencer, E.M., Liu, C.C., Si, E.C.C., and Howard, G.A. *In vivo* actions of insulin-like growth factor-I (IGF-I) on bone formation and resorption in rats. Bone **12,** 21, 1991.
36. Li, Y., Yu, X., Lin, S., Li, X., Zhang, S., and Song, Y-H. Insulin-lile growth factor 1 enhances the migratory capacity of mesenchymal stem cells. Biochem Biophys Res Commun **356,** 780, 2007.
37. Kaigler, D., Krebsbach, P.H., Polverini, P.J., and Moony, D.J. Role of vascular endothelial growth factor in bone marrow stromal cell modulation of endothelial cells. Tissue Eng **9,** 95, 2003.
38. Akeno, N., Robins, J., Zhang, M., Czyzyk-Krzeska, M.F., and Clemenc, T.L. Induction of vascular endothelial growth factor by IGF-1 in osteoblast-like cell is mediated by the PI3K signaling pathway through the hypoxia-inducible factor-2α. Endocrinology **143,** 420, 2002.
39. Riddle, R.C., Khatri, R., Schipani, E., and Clemens, T.L. Role of hypoxia-inducible factor-1α in angiogenic-osteogenic coupling. J Mol Med **87,** 583, 2009.
40. Kawasaki, K., Aihara, M., Honmo, J., Sakurai, S., Fujimaki, Y., Sakamoto, K., Fujimaki, E., Wozney, J.M., and Yamaguchi, A. Effects of recombinant human bone morphogenetic protein-2 on differentiation of cells isolated from human bone, muscle, and skin. Bone **23,** 223, 1998.
41. Shields, L.B., Raque, G.H., Glassman, S.D., Campbell, M., Vitaz, T., Harpring, J., and Shields, C.B. Adverse effects associated with high-dose recombinant human bone morphogenetic protein-2 use in anterior cervical spine fusion. Spine **31,** 542, 2006.
42. Stephan, S.J., Tholpady, S.S., Gross, B., Petrie-Aronin, C.E., Botchway, E.A., Nair, L.S., Ogle, R.C., and Park, S.S. Injectable tissue-engineered bone repair of a rat calvarial defect. Laryngoscope **120,** 895, 2010.
43. Maitra, B., Szekely, E., Gjini, K., Laughlin, M.J., Dennis, J., Haynesworth, S.E., and Koc, O.N. Human mesenchymal stem cells support unrelated donor hematopoietic stem cells and suppress T-cell activation. Bone Marrow Transplant **33,** 597, 2004.
44. Di Nicola, M., Carlo-Stella, C., Magni, M., Milanesi, M., Longoni, P.D., Matteucci, P., Grisanti, S., and Gianni, A.M. Human bone marrow stromal cells suppress T-lymphocyte proliferation induced by cellular or nonspecific mitogenic stimuli. Blood **99,** 3838, 2002.
45. Le Blanc, K., Tammik, L., Sundberg, B., Haynesworth, SE., and Ringdén, O. Mesenchymal stem cells inhibit and stimulate mixed lymphocyte cultures and mitogenic responses independently of the major histocompatibility complex. Scand J Immunol **57,** 11, 2003.
46. Bartholomew, A., Sturgeon, C., Siatskas, M., Ferrer, K., McIntosh, K., Patil, S., Hardy, W., Devine, S., Ucker, D., Deans, R., Moseley, A., and Hoffman, R. Mesenchymal stem cells suppress lymphocyte proliferation *in vitro* and prolong skin graft survival *in vivo*. Exp Hematol **30,** 42, 2002.

Address correspondence to:
Wataru Katagiri, D.D.S., Ph.D.
Department of Oral and Maxillofacial Surgery
Nagoya University Graduate School of Medicine
65 Tsuruma-cho, Showa-ku, Nagoya
Aichi 466-8550
Japan

E-mail: w-kat@med.nagoya-u.ac.jp

Received: June 8, 2011
Accepted: March 14, 2012
Online Publication Date: May 31, 2012

Cytotherapy, 2012; Early Online: 1–11

informa
healthcare

Mesenchymal stromal cells of human umbilical cord Wharton's jelly accelerate wound healing by paracrine mechanisms

RYUTARO SHOHARA[1], AKIHITO YAMAMOTO[1], SACHIKO TAKIKAWA[2], AKIRA IWASE[2], HIDEHARU HIBI[1], FUMITAKA KIKKAWA[2] & MINORU UEDA[1]

[1]*Department of Oral and Maxillofacial Surgery, and* [2]*Department of Obstetrics and Gynecology, Nagoya University Graduate School of Medicine, Nagoya, Japan*

Abstract

Background aims. Mesenchymal stromal cells (MSC) can be isolated from the perivascular connective tissue of umbilical cords, called Wharton's jelly. These human umbilical cord perivascular cells (HUCPVC) might provide therapeutic benefits when treating skeletal or cutaneous malformations in neonatal patients. *Methods.* HUCPVC were isolated, and their proliferation rate, marker expression and multilineage differentiation potential determined. HUCPVC or their conditioned medium (HUCPVC-CM) was injected into the excisional wound of a mouse splinted-wound model. The effects of the treatment on wound closure were examined by morphohistochemical and gene expression analyses. *Results.* HUCPVC expressed typical MSC markers and could differentiate into osteoblastic and adipogenic lineages. HUCPVC transplanted into the mouse wound accelerated wound closure. Immunohistologic analysis showed that the HUCPVC accelerated wound healing by enhancing collagen deposition and angiogenesis via paracrine mechanisms. Furthermore, treatment with HUCPVC-CM alone significantly enhanced wound closure. HUCPVC-CM increased the number of anti-inflammatory M2 macrophages expressing resistin-like molecule (RELM)-α/CD11b and promoted neovessel maturation. Quantitative polymerase chain reaction (PCR) analysis showed that HUCPVC-CM increased the expression of tissue-repairing cytokines interleukin (IL)-10, transforming growth factor (TGF)-β1, vascular endothelial growth factor (VEGF)-1 and angiopoietin-1 at the healing wound. *Conclusions.* Our results show that HUCPVC promotes wound healing via multifaceted paracrine mechanisms. Together with their ability to differentiate into the osteogenic linage, HUCPVC may provide significant therapeutic benefits for treating wounds in neonatal patients.

Key Words: *human umbilical cord perivascular cells, wound healing, mesenchymal stromal cells, anti-inflammatory M2 macrophage*

Introduction

Neonatal congenital disorders, such as cleft lip and palate, involve soft tissue defects as well as skeletal abnormalities. The clefts are closed surgically to allow for normal feeding and speech development; however, it is difficult to control post-surgical wound healing and cutaneous integrity. Thus the development of therapeutic approaches accelerating both skeletal regeneration and wound healing would be valuable for treating a variety of neonatal congenital abnormalities.

Wound healing is characterized by five sequential and partially overlapping phases: hemostasis, inflammation, cellular proliferation, angiogenesis and extracellular matrix (ECM) deposition (1). Dysfunctions in these phases frequently result in chronic wounds or ulcers (2). Recent studies have revealed that two types of tissue macrophages originating from peripheral blood monocytes play important roles in these healing processes (3–6). Classically activated M1 macrophages are stimulated with the T-helper (h)1 cytokines interferon (IFN)-γ and lipopolysaccharide (LPS). M1 macrophages secrete pro-inflammatory cytokines [tumor necrosis factor (TNF)-α, interleukin (IL)-1 and IL-6] and function in host defense against infection. The alternatively activated M2, or wound, macrophages are stimulated by the Th2 cytokines IL-4 and IL-13. M2 macrophages secrete the anti-inflammatory cytokine IL-10 and tissue-repairing factors transforming growth (TGF)-β and vascular endothelial growth factor (VEGF). The polarity of macrophages changes from M1 to M2 during the physiologic wound repair process (7–9). Thus strategies for promoting the M1/M2 transition may provide significant therapeutic benefits for treating severe wounds.

Correspondence: **Akihito Yamamoto**, DDS, PhD, Department of Oral and Maxillofacial Surgery, Nagoya University Graduate School of Medicine, 65 Tsuruma-cho, Showa-ku, Nagoya 466–8550, Japan. E-mail: akihito@med.nagoya-u.ac.jp

(Received 24 November 2011; accepted 21 June 2012)

ISSN 1465-3249 print/ISSN 1477-2566 online
DOI: 10.3109/14653249.2012.706705

Stem cell-based transplantation therapy holds promise as a strategy for promoting multiple tissue-healing processes. In the last decade, a variety of cell types, including adult human bone marrow (BM) mesenchymal stromal cells (BMMSC) (10–12), adipose mesenchymal stromal cells (MSC) (13,14), dental pulp MSC (15,16) and gingival mucosa MSC (17), has been transplanted into a mouse full-thickness skin excision model, and the regenerative activities evaluated. These pre-clinical studies have shown that the engrafted stem cells promote cutaneous wound healing through both cell-autonomous differentiation and paracrine effects. The paracrine factors generated by some of these MSC have been shown to promote M1/M2 transition, angiogenesis and cell proliferation (17–22). Thus MSC provide multifaceted therapeutic benefits for treating wound repair. However, especially for perinatal patients, the isolation of these stem cells requires an invasive operation, and the number of isolated stem cells is insufficient for treatment. Therefore it is important to identify an alternative source of stem cells that could promote wound healing in congenital disease patients.

The umbilical cord is a large organ, developing up to 30–60 cm in length during gestation. It is routinely discarded as medical waste after delivery. However, the perivascular connective tissue of umbilical cords is a rich source of MSC (23,24), called human umbilical cord perivascular cells (HUCPVC). HUCPVC exhibit multipotential differentiation activity and promote wound healing (25); however, the mechanisms underlying these biologic activities are still largely unknown. In this study, we show that HUCPVC promote wound healing via multifaceted paracrine mechanisms. Together with their ability to differentiate into the osteogenic linage, HUCPVC may provide significant therapeutic benefits for treating wounds in neonatal patients.

Methods

Isolation of HUCPVC and cell culture

The research protocol was approved by the ethics committee of Nagoya University School of Medicine (Nagoya, Japan). HUCPVC were isolated according to the method described by Sarugaser *et al.* (24) from the umbilical cords of consenting patients who underwent full-term Caesarian sections. The cells were maintained in a monolayer culture in low-glucose Dulbecco's modified Eagle's medium (DMEM; Sigma-Aldrich, St. Louis, MO), supplemented with 10% fetal bovine serum (FBS; PAA Laboratories GmbH, Pasching, Austria) and penicillin–streptomycin–amphotericin B (100 U/mL, 100 μg/mL and 0.25 μg/mL; Gibco, Grand Island, NY) at 37°C in 5% CO_2. MSC from three human BM lines (hBMMSC; from 20–22 year olds) at passage 3 and three human skin-fibroblast lines (hSFb; from 36–40 year olds) at passage 3 were obtained from (Lonza, Walkersville, MD) and the Health Science Research Resources Bank Japan, respectively. Cells from up to five passages were used in the subsequent experiments.

Cell-surface marker analysis

Cells were suspended in 100 μL phosphate-buffered saline (PBS) containing fluorescein isothiocyanate (FITC)-conjugated anti-human CD34 or CD45 (eBioscience Inc., Sandiego), phycoerythrin (PE)-conjugated anti-human CD73, CD105, HLA-DR (eBioscience Inc.) or CD90 (BD Pharmingen, San Jose, CA), or mouse monoclonal anti-human CD11b (BD Pharmingen). The cells were then incubated for 30 min at 4°C in the dark. The cells mixed with mouse monoclonal anti-human CD11b were washed in PBS and suspended in 100 μL PBS containing an FITC-conjugated anti-mouse IgG secondary antibody (Ab) (BD Pharmingen). The cells were then washed and analyzed with a FACSCalibur (BD Biosciences, San Jose, CA). Ten thousand events were analyzed by flow cytometry using Cell Quest (BD Biosciences) software.

Cell proliferation assays

Cells were plated at a density of 2.0×10^4 cells/mL/well in 12-well plates (Greiner Bio-One, Frickenhausen, Germany) in mesenchymal stromal cell growth medium (MSCGM: Lonza). The cell numbers were counted directly in triplicate, and the medium was replaced with fresh MSCGM on days 1 and 3.

Multilineage differentiation assays

To assess the osteogenic potential of HUCPVC, the cells were plated at 1.2×10^4 cells/well in a 12-well plate (Greiner Bio-One) in DMEM containing serum. Osteogenic induction medium, consisting of MSCGM supplemented with 100 nmol/L dexamethasone (Sigma-Aldrich), 10 mmol/L β-glycerophosphate (Merck KGaA, Darmstadt, Germany) and 0.2 mmol/L ascorbic acid-2-phosphate (Wako, Osaka, Japan), was added 24 h later. After 4 weeks of culture, the cells were stained with a saturated solution of Alizarin Red S (pH 4.2; Sigma-Aldrich). To evaluate the adipogenic potential of HUCPVC, the cells were plated at 8.0×10^4 cells/well in a 12-well plate (Greiner Bio-One) in DMEM containing serum, and the adipogenic induction medium from a kit (Lonza) was added after the culture reached confluence, according to the manufacturer's

Table I. Primers utilized in RT-PCR.

Gene	Forward sequence (5′–3′)	Reverse sequence (5′–3′)
GAPDH	AAGGTGAAGGTCGGAGTCAAC	GGGGTCATTGATGGCAACAATA
ALP	CCTCCTCGGAAGACACTCTG	GCAGTGAAGGGCTTCTTGTC
RUNX2	TTACTTACACCCCGCCAGTC	CAGACCAGCAGCACTCCATA
Osteocalcin	CACTCCTCGCCCTATTGGC	CCCTCCTGCTTGGACACAAAG

instructions. After 4 weeks of culture, the cells were stained with fresh Oil Red O solution (Sigma-Aldrich). Cells maintained in regular growth medium were used as a control.

Alkaline phosphatase activity assay

Cells were plated at a density of 6.0×10^3 cells/well in 24-well plates (Greiner Bio-One). After 24 h, 50, 100 or 300 ng/mL recombinant human bone morphogenetic protein (BMP)-2 (PeproTech, New Jersey, USA) were added to each well, and the cells were cultured for 7 more days. The medium was replaced with fresh medium containing the same amount of BMP-2 on day 4. After 7 days of incubation, the alkaline phosphatase (ALP) activity of the BMP-2-induced and non-induced HUCPVC was measured using a commercially available p-nitrophenyl phosphate tablet set (Sigma-Aldrich) and a cell-counting kit (WST-8s; Dojindo, Kumamoto, Japan), as described previously (26).

Reverse transcription–polymerase chain reaction

For RNA preparation, HUCPVC or hBMMSC were treated with or without 100 ng/mL BMP-2 for 14 days in 60-mm dishes. After 14 days of incubation, the total RNA was extracted with TRIzol reagent (Invitrogen, Carlsbad, CA). A total of 1 μg RNA was analyzed by reverse transcription (RT)–polymerase chain reaction (PCR) using Superscript III® reverse transcriptase and oligo-dT primers (Invitrogen), according to the manufacturer's protocol. Primer sets are listed in Table I. PCR was carried out with primers specific for ALP, runt-related transcription factor (RUNX)2, osteocalcin and glyceraldehyde-3-phosphate dehydrogenase (GAPDH). The amplified cDNA fragments were separated by electrophoresis through a 2% (wt/vol) agarose gel, stained with ethidium bromide, and photographed under an ultraviolet light transilluminator.

Quantitative real-time RT-PCR

Total RNA was extracted from 10 mm × 10 mm of excised skin tissue, including the wound and surrounding skin. Quantitative real-time RT-PCR was performed with a Stepone Plus (Applied Biosystems, Carlsbad, CA) and THUNDERBIRD qPCR mix (Toyobo, Osaka, Japan), according to standard protocols. Contamination of genomic DNA in the PCR reaction was checked by both melting curve and gel analyses of no-RT controls. Standard curves were generated for each gene, and the amplification was found to be 90–100% efficient. The relative quantification of gene expression was determined by comparison of threshold values. All the results were normalized to GAPDH. The primer sets are listed in Table II. The results are presented as the average of three replicate experiments. All the graphic data for mRNA expression are presented as the fold expression relative to the reference day 0, over time (days after transplantation).

Conditioned medium

Conditioned medium (CM) was generated as follows: 80% confluent passage 5 hSFb or HUCPVC in 10-cm tissue culture dishes were washed with PBS twice, then fed with 7 mL per dish serum-free DMEM and incubated for 48 h at 37°C in 5% CO_2. The CM were collected by centrifugation at 440 ***g*** for 5 min, and centrifuged again at 1750 ***g*** for 3 min to remove cell debris.

Table II. Primers utilized in quantitative real-time RT-PCR.

Gene	Forward sequence (5′–3′)	Reverse sequence (5′–3′)
GAPDH	AACTTTGGCATTGTGGAAGGT	GGATGCAGGGATGATGTTCT
IL-10	GCTCTTACTGACTGGCATGAG	CGCAGCTCTAGGAGCATGTG
RELM-α	CCAATCCAGCTAACTATCCCTCC	CCAGTCAACGAGTAAGCACAG
VEGF-1	GCACTGGACCCTGGCTTTAC	CTTCTGCTCTCCTTCTGTCGTG
Angiopoietin-1	CACATAGGGTGCAGCAACCA	CGTCGTGTTCTGGAAGAATGA
TGF-β1	CGCCTGAGTGGCTGTCTTT	CGTGGAGTTTGTTATCTTTGCTGT

Wound healing model and HUCPVC transplantation

The animal experiments were performed in accordance with the Guidelines for Animal Experimentation of Nagoya University School of Medicine. BALB/c nude mice (8 weeks old, female) and like a BALB/C (ICR) mice (8 weeks old, female) were used for the HUCPVC transplantation and CM injection, respectively. The excisional wound-splinting model was carried out as described previously, with modification (27). Briefly, the mice were anesthetized individually and 6-mm full-thickness excisional skin wounds were made on the dorsum, using a 6-mm tissue punch (Kai Industries Co., ltd., Gifu, Japan) and Iris scissors. Two wounds were created, one on each side of the midline. A donut-shaped splint with a diameter twice that of the wounds was made from 0.5-mm thick silicone sheet. A fast-bonding adhesive (Aron Alpha®; Toagosei, Tokyo, Japan) was used to fix the splint to the skin, followed by interrupted 4–0 nylon sutures to ensure its position.

The wounds were treated with HUCPVC or CM immediately after wound creation, as follows. The cultured HUCPVC and hSFb were detached from the culture dishes by enzymatic treatment with 0.05% trypsin/ethylenediaminetetraacetic acid (EDTA) and pre-labeled with PKH26 (Sigma-Aldrich), according to the manufacturer's protocol. Each wound received 1 million cells: 0.8×10^6 cells in 80 μL PBS were injected intradermally around the wound at four injection sites, and 0.2×10^6 cells in 20 μL PBS were applied to the wound bed. For the CM injection, 80 μL CM were injected around the wound and 20 μL CM were applied to the wound bed. After all the procedures, Tegaderm (3M, London, ON, Canada) was placed over the wound, and the animals were housed individually.

Wound analysis

Digital photographs of the wounds were taken on days 0, 4, 7, 10 and 14 after wounding. The wound area was analyzed by tracing the wound margin using image analysis software (ImageJ). The percentage of wound closure was calculated as follows: (area of original wound – area of wound at time of analysis)/ area of original wound × 100.

Histologic analysis

On day 4, 7 or 14 after the operation, the mice were killed and skin fragments, including the wound area and 4 mm of the surrounding skin, were dissected out using a scalpel and scissors, fixed in 4% paraformaldehyde, separated into two pieces at the midline, and embedded in OCT compound (Tissue-Tek, Miles Inc, Elkhart, IN). Six-micron thick frozen sections were prepared on a cryostat and stained with hematoxylin-eosin (HE) for light microscopy. For immunofluorescent staining, sections were fixed in 4% paraformaldehyde for 1 min at room temperature, washed, blocked with 5% bovine serum albumin/PBS for 30 min, and then incubated with primary Ab in blocking buffer for 1 h. The sections were incubated with secondary Ab for 30 min, mounted with PermaFluor Mountant (Thermo Scientific, Fremont, CA) and analyzed by fluorescence microscopy with a BZ9000 (Keyence, Osaka, Japan). The following Ab were used for immunostaining: rat monoclonal Ab (MAb) against CD31 (eBioscience) and CD11b (eBioscience), rabbit polyclonal Ab against α-smooth muscle actin (SMA) (Millipore, Billerica, MA) and resistin-like molecule (RELM)-α (Abcam, Cambridge, MA) and goat Ab against human type I collagen (Abcam). Secondary Ab were conjugated with Alexa Fluor 488 or 647 (Invitrogen). Cell nuclei were labeled with 4′, 6-diamidino-2-phenylindole dihydrochloride (DAPI; Invitrogen). Capillary density was assessed morphometrically by examining five fields per section of the wound between the edges in three successive sections after immunofluorescence staining using the anti-CD31 Ab.

Quantification and statistical analysis

To quantify the cells expressing a given marker or marker combination, we used ImageJ or a Dynamic cell counter (Keyence). All values are expressed as the mean ± SD. Comparisons of results between experimental groups and control groups were analyzed with a Student's *t*-test. Statistical analyses were performed using the SPSS version 19.0.0 software package. If the *P*-value was < 0.05, the result obtained was considered to be significant.

Results

Characterization of isolated HUCPVC

HUCPVC were isolated from the Wharton's jelly surrounding umbilical cord vessels as described elsewhere (24). They exhibited a fibroblastic morphology with a bipolar spindle shape (Figure 1A). The cell proliferation of the HUCPVC at the 5th passage was two times faster than that of hBMMSC of the same passage (Figure 1B). Flow cytometric analysis showed that the HUCPVC expressed high levels of the MSC markers (28) CD73, CD90 and CD105, but not the hematopoietic markers CD34, CD45, CD11b and HLA-DR (Figure 1C).

Next, we examined the differentiation potential of HUCPVC. In the osteogenic differentiation

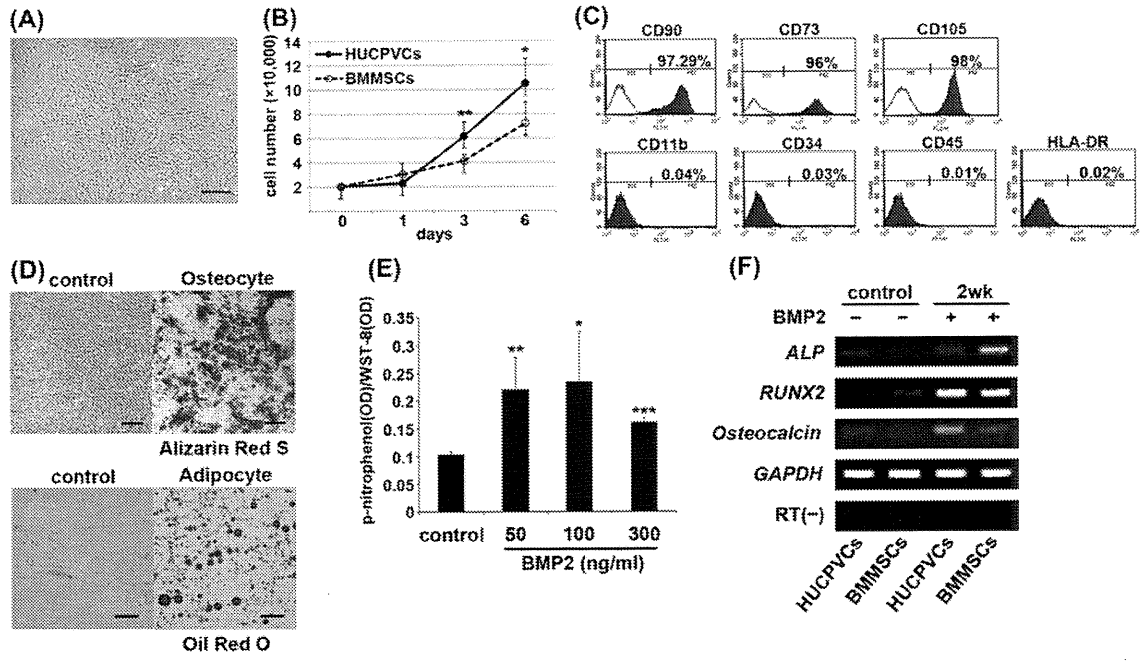

Figure 1. Characterization of isolated HUCPVC. (A) Morphology of HUCPVC. Scale bar = 200 μm. (B) Cell proliferation rate of the HUCPVC at the 5th passage ($n = 3$ for each time-point and group). (C) Representative image of the expression of cell-surface markers. (D) Multidifferentiation potential of HUCPVC. HUCPVC formed Alizarin Red-positive condensed nodules after 4 weeks in osteogenic induction medium. HUCPVC differentiated into Oil Red O-positive adipocytes after 4 weeks in adipogenic differentiation medium. Scale bar = 100 μm. (E) The level of ALP activity was significantly increased in HUCPVC treated with BMP-2 for 7 days ($n = 3$ for each group). (F) The expression of osteogenic differentiation markers RUNX2 and osteocalcin was examined by RT-PCR. Data are presented as means ± SD. $^{*}P < 0.05$; $^{**}P < 0.01$; $^{****}P < 0.001$.

medium, HUCPVC formed many Alizarin Red-positive condensed nodules (Figure 1D). Furthermore, HUCPVC treated with BMP-2 showed significantly increased ALP activity (Figure 1E) and expression of the osteogenic differentiation markers RUNX2 and osteocalcin (Figure 1F). In the adipogenic differentiation medium, many of the HUCPVC differentiated into Oil Red O-positive adipocytes (Figure 1D). Taken together, these results demonstrated that the isolated HUCPVC comprised a highly proliferative multipotent MSC-like population.

Transplanted HUCPVC accelerated wound healing

To investigate the wound-repair activity of HUCPVC, we transplanted them into a mouse excisional splinted-wound model (Figure 2A) and examined the rate of wound closure. We found that the wounds receiving the HUCPVC exhibited significantly faster healing compared with the hSFb-treated and PBS-injected controls (Figure 2B). Importantly, the superior healing of the HUCPVC-treated group was evident soon after treatment (4 days post-operation) (Figure 2C). At 14 days after the operation, the area of wound closure was 99.72 ± 0.17% in the HUCPVC-treated group, 88.75 ± 0.46% in the hSFb-treated group, and 82.13 ± 5.85% in the control group.

Histologic analysis of the wounds on day 14 showed that the granulation tissue of the HUCPVC-treated group appeared thicker and covered a larger area than that of the hSFb-treated and PBS groups (Figure 2D,H,L). Immunohistologic analysis with an anti-human type I collagen MAb showed that the engrafted HUCPVC generated packed collagen bundles (Figure 2M,N). Staining with an anti-mouse CD31 MAb, a marker for endothelial-cell lineages, revealed that the transplanted HUCPVC promoted endothelial-cell recruitment (Figure 2O). This recruitment was marginal in the hSFb and PBS groups (Figure 2G,K). Although we examined the contribution of transplanted PKH26-labeled HUCPVC to the skin tissue, none of the labeled cells expressed CD31 or differentiated into the typical cutaneous resident cells (data not shown). Taken together, these results suggested that the HUCPVC accelerated wound healing through the enhancement of collagen deposition and angiogenesis via paracrine mechanisms.

CM derived from HUCPVC enhanced wound healing and neovascular network formation

To examine further the roles of paracrine activity in the HUCPVC-promoted wound healing, a total of

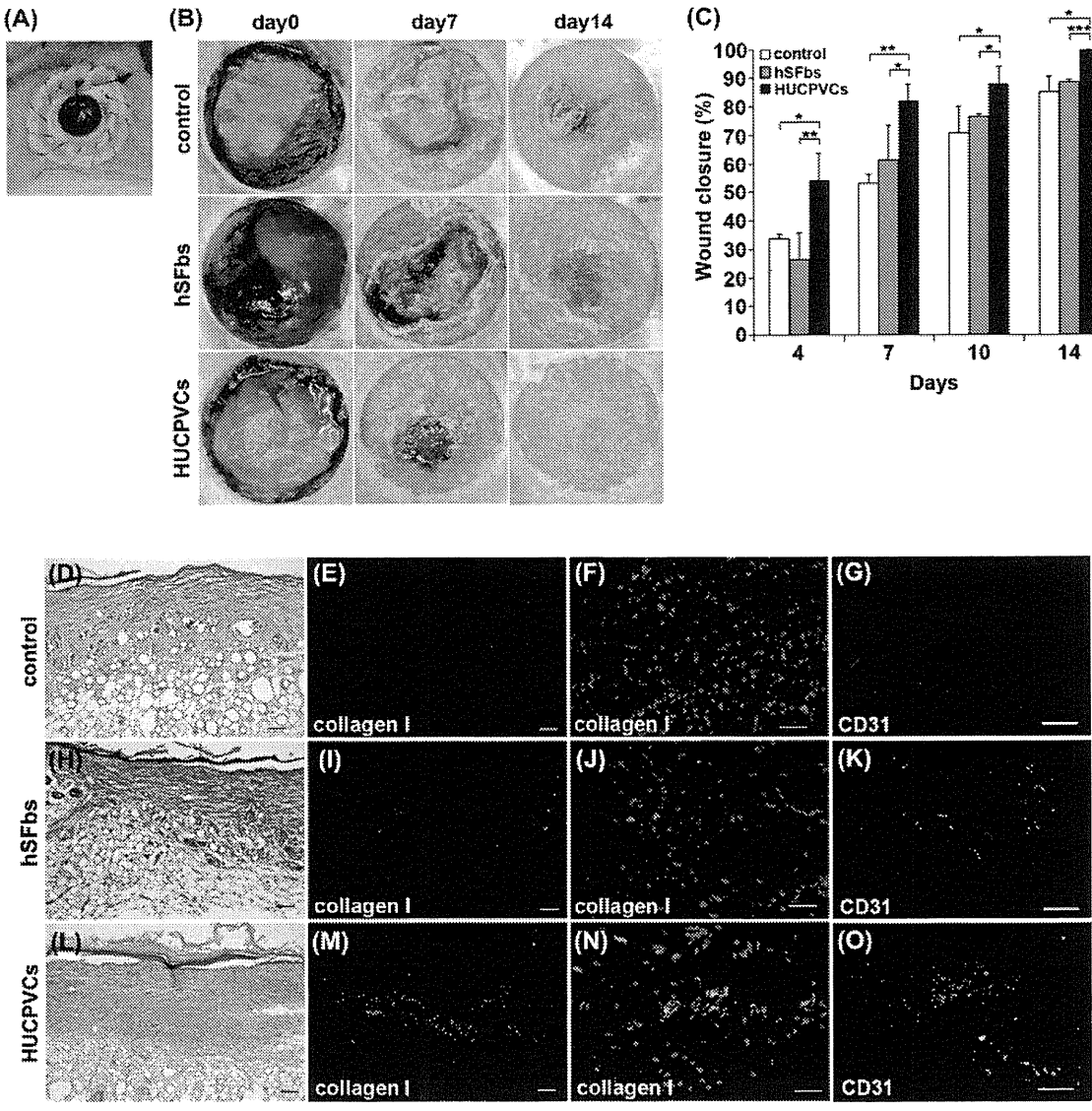

Figure 2. Transplanted HUCPVC accelerated wound healing. (A) Mouse excisional wound-splinting model. (B) Representative photographs of the wounds on days 7 and 14 after HUCPVC transplantation. (C) Measurement of wound closure at different time-points (HUCPVC, $n = 6$; hSFb, $n = 6$; PBS, $n = 10$). The percentage of wound closure was calculated as: (area of original wound – area of wound at time of analysis)/area of original wound × 100. (D–O) Histologic analysis of the wound 14 days after transplantation. (D, H, L) HE staining. (E, F, I, J, M, N) Staining with an anti-human type I collagen MAb. (G, K, O). Staining with an anti-mouse CD31 MAb. Scale bar = 100 μm. Controls were PBS-injected. Data are presented as means ± SD. $^{*}P < 0.05$; $^{**}P < 0.01$; $^{***}P < 0.001$.

100 μL serum-free CM from cultured HUCPVC or human skin fibroblasts (hSFb) was injected into four sites surrounding the wound and applied to the wound bed. As shown in Figure 3A, wounds receiving HUCPVC-CM healed faster than the PBS-treated control or hSFb-CM groups. Quantitative analysis showed that the closed wound area of the HUCPVC-CM group was significantly larger than that of the control or hSFb-CM group at both 4 and 7 days post-operation (Figure 3B).

We next examined whether HUCPVC-CM promotes the formation of mature vessels composed of two types of cells, $CD31^{+}$ endothelial cells and α-SMA^{+} pericytes. Endothelial cells line the vessel lumen as a continuous layer, while pericytes, which are of mesenchymal origin, constitute the outer layer of microvessels (29,30). The pericytes play important roles in vessel maturation, remodeling and the stabilization of neovessels. We found many tubular microvessel structures composed of both $CD31^{+}$ and α-SMA^{+} cell layers in wounds treated with HUCPVC-CM at 7 days post-operation (Figure 3C). Quantitative analysis showed that the capillary density significantly increased in the HUCPVC-CM

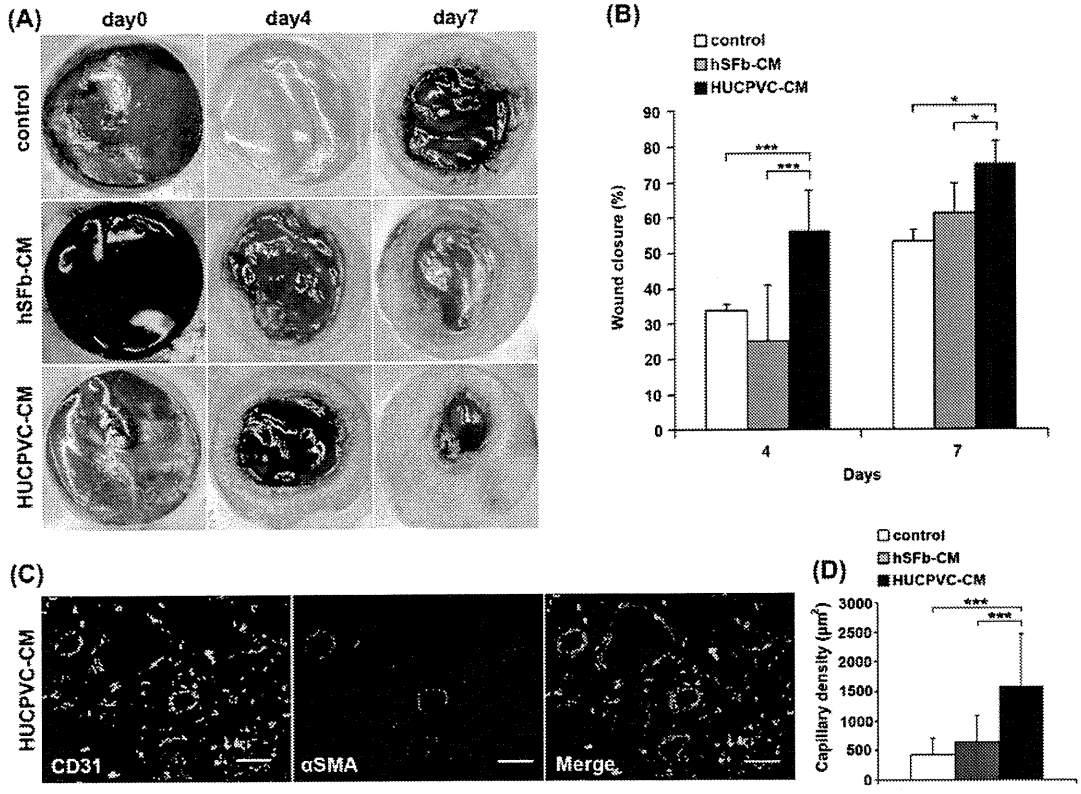

Figure 3. CM derived from HUCPVC-enhanced wound healing and neovascular network formation. (A) Representative photographs of the wounds 4 and 7 days after injection of the CM from HUCPVC, CM from hSFb or PBS. (B) Measurement of wound closure on days 4 and 7 (HUCPVC-CM, $n = 6$; hSFb-CM, $n = 6$; PBS, $n = 10$). The closed wound area of the HUCPVC-CM group was significantly larger than that of the control or hSFb-CM group. (C) Representative image of the immunohistochemical staining for CD31 (green) and α-SMA (red). Many tubular microvessel structures composed of both $CD31^+$ and $\alpha\text{-SMA}^+$ cell layers were observed in the wound treated with HUCPVC-CM. Scale bar = 50 μm. (D) Capillary density in wounds on day 7 was measured after CD31 and α-SMA staining ($n = 3$ wounds on three mice for each group). The capillary density was significantly increased in the HUCPVC-CM group compared with the control. Data are presented as means ± SD. $^*P < 0.05$; $^{***}P < 0.001$.

group compared with hSFb-CM group and the control (Figure 3D). These results demonstrated that paracrine factors in the HUCPVC-CM promoted vessel maturation and wound-healing processes.

HUCPVC-CM increased the number of anti-inflammatory M2 macrophages

Anti-inflammatory M2 macrophages expressing RELM-α and CD11b are known to play a pivotal role in wound healing (3,17). To investigate whether HUCPVC-CM affected the polarity of macrophages, we immunohistochemically analyzed the ratio of cells expressing RELM-α, a specific marker for M2 macrophages, versus CD11b, a common marker for monocytes and macrophages. We found that HUCPVC-CM treatment increased the number of cells positive for both RELM-α and CD11b (Figure 4A). Quantitative analysis revealed that the percentages of $\text{RELM-}\alpha^+$ cells in the $CD11b^+$ population in the HUCPVC-CM-treated, hSFb-CM-treated and PBS-treated groups were 46.5 ± 6.3%, 17.4 ± 3.3% and 22.7 ± 4.5% on day 4, and 54.3 ± 8.0%, 29.2 ± 4.4% and 31.2 ± 7.7% on day 7, respectively (Figure 4B). These results suggested that HUCPVC-CM contains some factors that are involved in activating the M2 macrophages.

HUCPVC-CM activated endogenous tissue repair activity

We further examined the effects of local HUCPVC-CM administration on wound healing by quantitative real-time PCR analysis. RNA was extracted from the wound tissues and from the surrounding area at 0, 1, 4 and 7 days post-operation. HUCPVC-CM treatment increased the expression of RELM-α, confirming the immunohistologic data (Figure 5A). Importantly, HUCPVC-CM treatment also up-regulated the expression of four major tissue-repairing

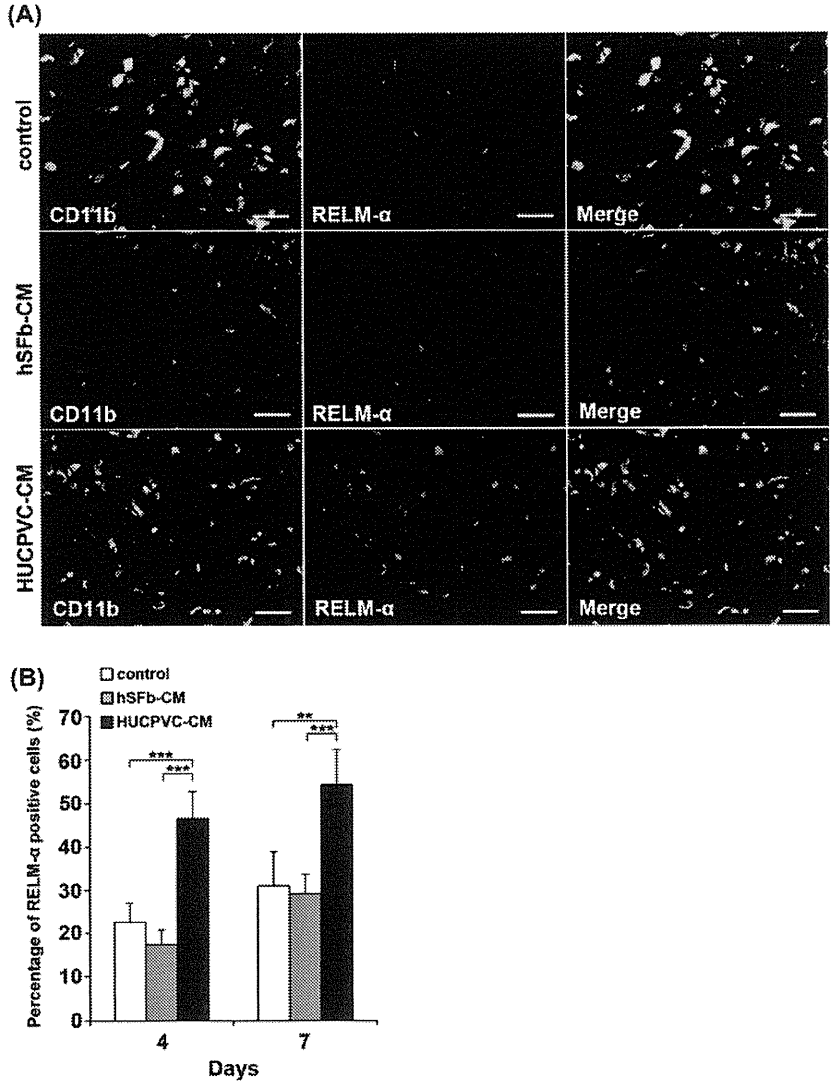

Figure 4. HUCPVC-CM increased the number of anti-inflammatory M2 macrophages. (A) Immunohistologic staining with CD11b (green) and RELM-α (red) on day 4 after HUCPVC-CM injection. The control was PBS-injected. Scale bar = 50 μm. (B) Quantitative analysis of the percentage of RELM-α^+ M2 macrophages in the CD11b$^+$ population. Data are presented as the means ± SD; $n = 3$ wounds on three mice for each time-point. $^{**}P < 0.01$; $^{***}P < 0.001$.

factors: (a) IL-10, an anti-inflammatory cytokine expressed by M2 macrophages, (b) TGF-β1, a main regulator of myofibroblast differentiation and granulation tissue formation, (c) VEGF-1, a factor that promotes the differentiation of endothelial precursors and their sprouting, and (d) angiopoietin-1, a ligand of the Tie2 receptor that promotes neovessel maturation (Figure 5B–E). In contrast, we found little or no effect of hSFb-CM or PBS on the expression of tissue-repairing genes. Taken together, these results demonstrated that paracrine factors derived from the HUCPVC activated endogenous tissue-repairing machineries via paracrine mechanisms.

Discussion

In this study, we characterized HUCPVC *in vitro* and examined their therapeutic benefits in a rodent wound-healing model. Our results revealed that the HUCPVC are a highly proliferative MSC-like population that exhibits multipotent differentiative capacity (i.e. in the osteoblastic and adipogenic lineages). When transplanted into the mouse full-thickness excisional splinted-wound model, HUCPVC accelerated the healing process through the activation of tissue-repairing/M2 macrophages and the promotion of granulation tissue formation, re-epithelialization,

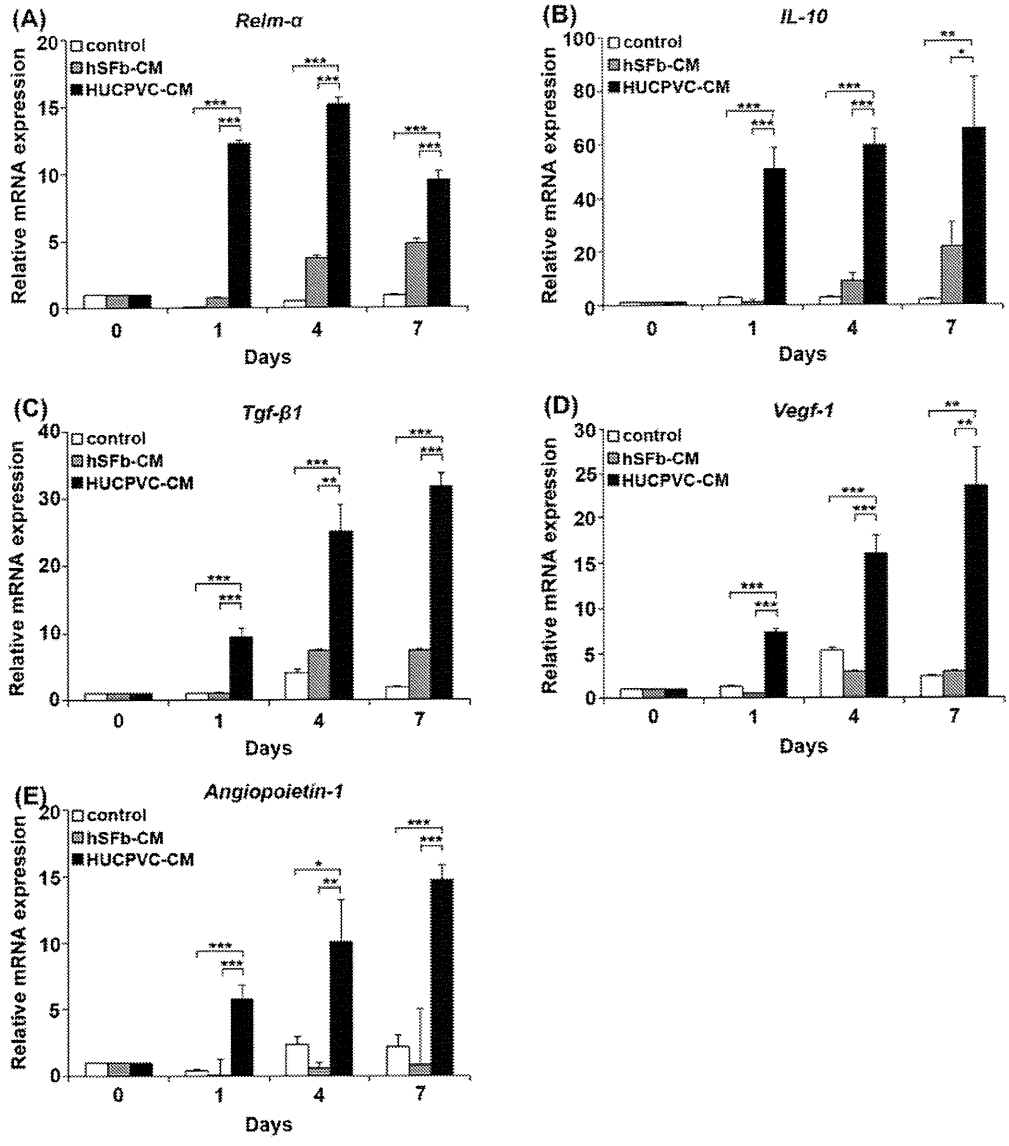

Figure 5. HUCPVC-CM-activated endogenous tissue repair activity. (A–E) Quantitative real-time PCR of RELM-α, IL-10, TGF-β1, VEGF-1 and angiopoietin-1. The RNA was isolated from the wounds on days 0, 1, 4 and 7 post-operation. Data are presented as the means ± SD; $n = 3$. $^{*}P < 0.05$; $^{**}P < 0.01$; $^{***}P < 0.001$.

neovascularization and collagen matrix deposition. Importantly, our data indicate that HUCPVC exert these multifaceted wound-healing activities via paracrine mechanisms.

Recent studies have highlighted the essential roles of the anti-inflammatory M2 macrophages in tissue repair and regeneration (3–5,7–9,17,31). The selective ablation of macrophages in a mouse wound model results in delayed re-epithelialization, decreased collagen deposition and impaired angiogenesis (32,33). These impaired tissue-repairing activities are associated with decreased production of TGF-β1 and VEGF from M2 macrophages (32,33). Our data showed that HUCPVC-CM increased remarkably the number of RELM-α^{+}/CD11b^{+} M2 macrophages in the peri-wound region at both 4 and 7 days post-operation (Figure 4B). This M2 activation was associated with an increased expression of anti-inflammatory cytokine IL-10 and tissue-repairing cytokines TGF-β1 and VEGF (Figure 5B–D). Thus our data demonstrate that HUCPVC modulate endogenous wound-healing events through the activation of anti-inflammatory/tissue-repairing M2 macrophages.

It is well established that Th1 cell-derived IL-4 and IL-13 are typical inducers of M2 macrophages

(5,6). In addition, recent studies have revealed other M2 inducers, including IL-10 (34), granulocyte–macrophage colony-stimulating factor (GM-CSF) (35–37), prostaglandin E2 (38,39), CC Chemokine Ligand (CCL)2 and IL-6 (40). Although the paracrine factors in HUCPV-CM involved in the M2 activation are currently unknown, in a preliminary gene expression analysis we found that HUCPVC expressed most of these M2 inducers, except for IL-4 and IL-13 (data not shown). Future global proteome analysis of HUCPVC-CM may clarify the factors and mechanisms by which HUCPVC activate M2 macrophages. In this study, we examined the tissue regeneration activity of HUCPV-CM by injecting them into the ICR wound model. To distinguish the immune-regulatory role of CM, we used hSFb-CM as a cellular control. We believe that our data reveal the different tissue-regenerating activities between these two types of cells.

Neovascularization is prerequisite for tissue repair and maintenance. New vessel formation consists of two sequential phases: vasculogenesis and angiogenesis. Vasculogenesis involves the recruitment of endothelial progenitor cells and their differentiation into mature endothelial cells. Angiogenesis involves the sprouting and remodeling of the primitive vessels, and the subsequent stabilization of the sprouts by mural cells (pericytes in medium-sized vessels and smooth muscle cells in larger ones). The interaction between endothelial cells and mural cells stabilizes microvessels and prevents vessel leakage, and thus is required for vessel maturation (29,30). Our results showed that HUCPVC promoted both vasculogenesis and angiogenesis via paracrine mechanisms. The formation of mature microvessels was significantly increased in the HUCPVC-CM-treated group compared with controls. In addition, HUCPVC-CM injection activated the local gene expression of vascular endothelial growth factor (VEGF)-a and angiopoietin-1 at the wound area. VEGF induces endothelial cell migration and proliferation and initiates blood-vessel formation (41). Angiopoietin-1 mediates neovessel maturation into more complex and larger vascular structures and maintains vessel integrity through the recruitment of mural cells (41). Thus HUCPVC promote neovascularization, at least in part, by activating endogenous angiogenic machinery. We also found many α-SMA$^+$ cells that were not involved in the microvessel structure. We speculate that these cells represent myofibroblasts recruited into the healing wound. These cells may play an important role in the granulation tissue formation in the wound.

The current treatments for chronic wounds, including debridement, pressure offloading, compression, irrigation, warming, antibiotics, negative pressure and growth factors, do not resolve a variety of pathogeneses of the healing processes; therefore, they exhibit only modest therapeutic benefits. Here, we demonstrated that engrafted HUCPVC elicit multifaceted therapeutic benefits for the treatment of cutaneous injury. We propose that HUCPVC may be a promising cell source for the treatment of wound healing.

There are many reports describing the clinical benefits of BMMSC in wound treatment (10–12). However, BMMSC isolation is too invasive for neonates. The advantage of HUCPVC is that they can be isolated from the patient's umbilical cord, which is usually discarded as medical waste. Thus autologous HUCPVC can be isolated completely non-invasively. We think this is the greatest advantage of HUCPVC compared with other MSC. We believe that our findings will contribute to the development of new wound-healing therapies for newborn patients.

Acknowledgments

The authors thank Drs Akihiro Yajima, Masahito Fujio and Kiyoshi Sakai, and Ms Mami Naruse, for their encouragement to complete this study. We thank the Division of Experimental Animals and Medical Research Engineering, Nagoya University Graduate School of Medicine, for the housing of mice. This work was supported by Grants-in-Aid for Scientific Research on Priority Areas from the Ministry of Education, Culture, Sports, Science and Technology of Japan and the COE for education and research of the Micro-Nano Mechatronics Nagoya University Global COE Program.

Declaration of interest: The authors report no conflicts of interest. The authors alone are responsible for the content and writing of the paper.

References

1. Singer AJ, Clark RA. Cutaneous wound healing. N Engl J Med. 1999;341:738–46.
2. Eming S, Hammerschmidt M, Krieg T, Roers A. Interrelation of immunity and tissue repair or regeneration. Sem Cell Devel Biol. 2009;20:517–27.
3. Brancato SK, Albina JE. Wound macrophages as key regulators of repair origin, phenotype, and function. Am J Pathol. 2011;178:19–25.
4. Ricardo SD, van Goor H, Eddy AA. Macrophage diversity in renal injury and repair. J Clin Invest. 2008;118:3522–30.
5. Mosser DM, Edwards JP. Exploring the full spectrum of macrophage activation. Nat Rev Immunol. 2008;8:958–69.
6. Gordon S. Alternative activation of macrophages. Nat Rev Immunol. 2003;3:23–35.
7. Troidl C, Mollmann H, Nef H, Masseli F, Voss S, Szardien S, et al. Classically and alternatively activated macrophages contribute to tissue remodelling after myocardial infarction. J Cell Mol Med. 2009;13:3485–96.

8. Bystrom J, Evans I, Newson J, Stables M, Toor I, van Rooijen N, et al. Resolution-phase macrophages possess a unique inflammatory phenotype that is controlled by cAMP. Blood. 2008;112:4117–27.
9. Deonarine K, Panelli MC, Stashower ME, Jin P, Smith K, Slade HB, et al. Gene expression profiling of cutaneous wound healing. J Transl Med. 2007;5:11.
10. Imaizumi T, Akita S, Akino K, Hirano A. Acceleration of sensory neural regeneration and wound healing with human mesenchymal stem cells in immunodeficient rats. Stem Cells. 2007;25:2956–63.
11. Falanga V, Iwamoto S, Chartier M, Yufit T, Butmarc J, Kouttab N, et al. Autologous bone marrow-derived cultured mesenchymal stem cells delivered in a fibrin spray accelerate healing in murine and human cutaneous wounds. Tissue Eng. 2007;13:1299–312.
12. Fu X, Fang L, Li X, Cheng B, Sheng Z. Enhanced wound-healing quality with bone marrow mesenchymal stem cells autografting after skin injury. Wound Repair Regen. 2006;14: 325–35.
13. Amos PJ, Kapur SK, Stapor PC, Shang HL, Bekiranov S, Khurgel M, et al. Human adipose-derived stromal cells accelerate diabetic wound healing: impact of cell formulation and delivery. Tissue Engineering Part A. 2010;16:1595–606.
14. Kim WS, Park BS, Sung JH, Yang JM, Park SB, Kwak SJ, et al. Wound healing effect of adipose-derived stem cells: a critical role of secretory factors on human dermal fibroblasts. J Dermatol Sci. 2007;48:15–24.
15. Nishino Y, Yamada Y, Ebisawa K, Nakamura S, Okabe K, Umemura E, et al. Stem cells from human exfoliated deciduous teeth (SHED) enhance wound healing and the possibility of novel cell therapy. Cytotherapy. 2011;13:598–605.
16. Nishino Y, Ebisawa K, Yamada Y, Okabe K, Kamei Y, Ueda M. Human deciduous teeth dental pulp cells with basic fibroblast growth factor enhance wound healing of skin defect. J Craniofac Surg. 2011;22:438–42.
17. Zhang QZ, Su WR, Shi SH, Wilder-Smith P, Xiang AP, Wong A, et al. Human gingiva-derived mesenchymal stem cells elicit polarization of m2 macrophages and enhance cutaneous wound healing. Stem Cells. 2010;28:1856–68.
18. Wu Y, Zhao R, Tredget E. Concise review. Bone marrow-derived stem/progenitor cells in cutaneous repair and regeneration. Stem Cells. 2010;28:905–15.
19. Lee EY, Xia Y, Kim WS, Kim MH, Kim TH, Kim KJ, et al. Hypoxia-enhanced wound-healing function of adipose-derived stem cells: increase in stem cell proliferation and up-regulation of VEGF and bFGF. Wound Repair Regen. 2009;17:540–7.
20. Herdrich B, Lind R, Liechty K. Multipotent adult progenitor cells: their role in wound healing and the treatment of dermal wounds. Cytotherapy. 2008;10:543–50.
21. Chen L, Tredget E, Wu P, Wu Y. Paracrine factors of mesenchymal stem cells recruit macrophages and endothelial lineage cells and enhance wound healing. PLoS One. 2008;3:e1886.
22. Wu Y, Chen L, Scott P, Tredget E. Mesenchymal stem cells enhance wound healing through differentiation and angiogenesis. Stem Cells. 2007;25:2648–59.
23. Baksh D, Yao R, Tuan RS. Comparison of proliferative and multilineage differentiation potential of human mesenchymal stem cells derived from umbilical cord and bone marrow. Stem Cells. 2007;25:1384–92.
24. Sarugaser R, Lickorish D, Baksh D, Hosseini MM, Davies JE. Human umbilical cord perivascular (HUCPV) cells: a source of mesenchymal progenitors. Stem Cells. 2005;23:220–9.
25. Zebardast N, Lickorish D, Davies JE. Human umbilical cord perivascular cells (HUCPVC): a mesenchymal cell source for dermal wound healing. Organogenesis. 2010;6:197–203.
26. Agata H, Kagami H, Watanabe N, Ueda M. Effect of ischemic culture conditions on the survival and differentiation of porcine dental pulp-derived cells. Differentiation. 2008;76: 981–93.
27. Galiano RD, Michaels J, Dobryansky M, Levine JP, Gurtner GC. Quantitative and reproducible murine model of excisional wound healing. Wound Repair Regen. 2004;12:485–92.
28. Dominici M, Le Blanc K, Mueller I, Slaper-Cortenbach I, Marini F, Krause D, et al. Minimal criteria for defining multipotent mesenchymal stromal cells. The International Society for Cellular Therapy position statement. Cytotherapy. 2006;8:315–7.
29. Armulik A, Abramsson A, Betsholtz C. Endothelial/pericyte interactions. Circ Res. 2005;97:512–23.
30. Gerhardt H, Betsholtz C. Endothelial–pericyte interactions in angiogenesis. Cell Tiss Res. 2003;314:15–23.
31. Daley JM, Brancato SK, Thomay AA, Reichner JS, Albina JE. The phenotype of murine wound macrophages. J Leukocyte Biol. 2010;87:59–67.
32. Lucas T, Waisman A, Ranjan R, Roes J, Krieg T, Muller W, et al. Differential roles of macrophages in diverse phases of skin repair. J Immunol. 2010;184:3964–77.
33. Mirza R, DiPietro LA, Koh TJ. Selective and specific macrophage ablation is detrimental to wound healing in mice. Am J Pathol. 2009;175:2454–62.
34. Park-Min KH, Antoniv TT, Ivashkiv LB. Regulation of macrophage phenotype by long-term exposure to IL-10. Immunobiology. 2005;210:77–86.
35. Kuroda E, Ho V, Ruschmann J, Antignano F, Hamilton M, Rauh MJ, et al. SHIP represses the generation of IL-3-induced M2 macrophages by inhibiting IL-4 production from basophils. J Immunol. 2009;183:3652–60.
36. Chen GH, Olszewski MA, McDonald RA, Wells JC, Paine R, Huffnagle GB, et al. Role of granulocyte macrophage colony-stimulating factor in host defense against pulmonary Cryptococcus neoformans infection during murine allergic bronchopulmonary mycosis. Am J Pathol. 2007;170:1028–40.
37. Grant V, King AE, Faccenda E, Kelly RW. PGE/cAMP and GM-CSF synergise to induce a pro-tolerance cytokine profile in monocytic cell lines. Biochem Biophys Res Co. 2005;331:187–93.
38. Maggini J, Mirkin G, Bognanni I, Holmberg J, Piazzon IM, Nepomnaschy I, et al. Mouse bone marrow-derived mesenchymal stromal cells turn activated macrophages into a regulatory-like profile. PLoS One. 2010;5:e9252.
39. Nemeth K,* Leelahavanichkul A, Yuen PST, Mayer B, Parmelee A, Doi K, et al. Bone marrow stromal cells attenuate sepsis via prostaglandin E(2)-dependent reprogramming of host macrophages to increase their interleukin-10 production. Nat Med. 2009;15:42–49.
40. Roca H, Varsos ZS, Sud S, Craig MJ, Ying C, Pienta KJ. CCL2 and interleukin-6 promote survival of human CD11b$^+$ peripheral blood mononuclear cells and induce M2-type macrophage polarization. J Biol Chem. 2009;284:34342–54.
41. Fam NP, Verma S, Kutryk M, Stewart DJ. Clinician guide to angiogenesis. Circulation. 2003;108:2613–8.

Official Journal of TESMA
Regenerative Research
www.regres.tesma.org.my
E-ISSN 2232-0822
Tissue Engineering and Regenerative Medicine Society of Malaysia

Regenerative Research 1(2) 2012 39-48

PARADIGM SHIFT IN TISSUE ENGINEERED BONE

Ueda M*, Katagiri W

Department of Oral and Maxillofacial Surgery, Nagoya University
Graduate School of Medicine, Nagoya, Japan.

ARTICLE INFO

Submitted: 06-11-2012
Accepted: 08-11-2012
*Corresponding Author: Minoru Ueda, DDS, PhD

Email:mueda@med.nagoya-u.ac.jp

KEYWORDS

Tissue Engineering,
Bone,
Stem cells,
MSC,
Secretome,
Cytokine,
Sinus floor elevation,
Dental implant

ABSTRACT

The tremendous need for bone tissue in numerous clinical situations and the limited availability of suitable bone grafts are driving the development of new approaches to bone repair. We have developed tissue-engineered bone using autogenous bone marrow derived mesenchymal stem cells and platelet-rich plasma for dental implant surgery. Twenty-two sinus floor augmentation cases with tissue-engineered bone for dental implant treatment were performed and eighty-seven dental implants were installed to the regenerated area. Radiographic assessments showed 8.7 mm mean increase in mineralized tissue one year after the first surgery. Histomorphometric analysis was performed in 5 cases from the specimen obtained at the implant placement after 6 months. The average area of newly regenerated bone was 41.9% although there seemed to be no correlation between the bone area and the number of the transplanted cells. The tissue-engineered bone will be a promising technique for bone regeneration, but the fate of the transplanted cell was still unknown. We discuss the paracrine effect of the stem cells for bone regeneration. This paper indicates the "paradigm shift" in tissue-engineered bone.

1.0 Introduction

The tremendous need for bone tissue in numerous clinical situations and the limited availability of suitable bone grafts are driving the development of new approaches to bone repair. In the past the "gold standard" bone graft materials is autologous bone and this is limited in supply and its harvesting is associated with significant morbidity (Laurie *et al.*, 1984; Quarto *et al.*, 2001). Approximately 8%of iliac grafts result in major complications such as infection, blood loss, nerve injury, short- and long-term pain and functional deficit. The use of allografts avoids donor site issues but these grafts are associated with risks of infection and possible immune response of the most tissue (Stevenson, 1987),which can lead to high rates of complications (Alman *et al.*, 1995; Lord *et al.*, 1988; Mankin *et al.*, 1987). Thus, there is a trend toward tissue engineering as an alternative to the traditional techniques in bone repair. Langer and Vacanti defined tissue engineering as "an interdisciplinary field that applies the principles of engineering and life sciences toward the development of biological substitutes that restore, maintain, or improve tissue function or a whole organ (Langer *et al.*, 1993)". Regeneration of the bone tissue is the most studied field in tissue engineering. According to the concept, equivalents of the bone tissue can be obtained by targeted osteogenic differentiation of multipotent mesenchymal stem cells (MSC) of the bone marrow (BM). MSC pre differentiated towards osteogenic lineage are applied on biocompatible materials maintaining osteo induction and possessing sufficient osteo conductive properties (Hattori *et*

al., 2004) transplanted into the bone defect area. Creation of bone equivalents is now beyond the scope of numerous experimental studies about the possibility of effective reconstruction of the bone tissue using various biodegradable material and MSC (Fang *et al.*, 2007; Lendeckel *et al.*, 2004; Weinzierl *et al.*, 2006).

We have developed tissue-engineered bone for implant surgery because bone availability is the key to successful placement of endosseous implants and tissue-engineered bone is thought to be most effective in such a procedure (Ueda *et al.*, 2005; Yamada *et al.*, 2004). Twenty-two sinus floor augmentation cases with tissue-engineered bone for implant treatment were performed at the department of Oral and Maxillofacial Surgery in Nagoya University Hospital. We could regenerate bone in a sinus floor with minimal invasiveness and good plasticity, and to provide a clinical alternative to the previous graft materials. In our method, the cells were cultured in the presence of autoserum, induced into osteogenic cells and transplanted with autologous platelet rich plasma. The results of our study showed that tissue engineered bone using autologous bone marrow stromal cells was feasible for patients with severely atrophic maxilla and for sinus floor augmentation surgery.

However, this procedure suffers from some problems such as high capital investment, expensive cell culture, complicated safety and quality management issues regarding cell handling, and invasiveness of the procedure that is required for the collection of bone marrow MSCs and PRP from the patients. Moreover, recent studies of MSC transplantation in spinal cord injury revealed that the implanted MSCs did not survive for a long time (Ide *et al.*, 2010).Additionally, it is well established that MSCs secrete a variety of growth factors and cytokines (Chen *et al.*, 2008).These finding suggests that MSC is not a main player for bone regeneration but the paracrine effects of growth factors and cytokines secreted from the implanted MSCs may promote tissue repair and regeneration.

In this paper, we present the clinical results of bone regeneration with MSC and implant success rate after functional loading, peri-implant tissues of titanium fixtures that had been placed in regions augmented using the tissue-engineered bone. Then we approached to the mechanism of bone regeneration after MSC transplantation using our clinical data such as the correlation between number of cell and new bone. Finally we will propose a new concept in bone tissue engineering that is the paradigm shift in tissue-engineered bone.

2.0 Materials and Methods

2.1 Cell preparation

Mesenchymal stem cells were isolated from the patient's iliac crest marrow aspirates (10 mL) according to the reported method (Pittenger *et al.*, 1999). Briefly, the basal medium, low-glucose Dulbecco's Modified Eagle's Medium, and growth supplements (50 mL of serum, 10 mL of 200 mML glutamine,and 0.5 mL of penicillin–streptomycin mixture containing 25units of penicillin and 25 g of streptomycin) were purchased from Lonza Inc. (Walkersville, MD). Three supplements, dexamethasone, sodium glycerophosphate, and L-ascorbic acid 2-phosphate, for inducing osteogenesis were purchased from Sigma Chemical Co. (St. Louis, MO).The cells were incubated at 37°C in a humidified atmosphere containing95% air and 5% CO^2. The MSCs were replated at densities of $3.1x10^3$cells/cm^2 in 0.2 mL/cm^2 of control medium. The differentiated MSCs were confirmed by detecting alkaline phosphatase activity using p-nitrophenylphosphatase as a substrate. In culture, MSCs were trypsinized and used for implanting. For the safety of cultured cell, the culture media were examined for contaminations of bacterium, fungus, and mycoplasma before transplantation.

2.2 Platelet-rich plasma preparation

Preoperative hematological assessments included a complete blood count with platelet levels. The resulting pellet of platelets (PRP) was extracted one day before surgery. The PRP was isolated in a 200-mL-collection bag containing the anticoagulant citrate under a sterilized condition at the blood transfusion service department of Nagoya University Hospital, Japan. Briefly, the blood was first centrifuged for 10 minutes at350g. Subsequently, the yellow plasma containing the buffy coat, which contained the platelets and leukocytes, was removed. A second centrifugation at 3500g for 10 minutes was performed to combine the platelets into a single pellet and the plasma supernatant, which was platelet poor plasma and contained relatively few cells, was removed. The buffy coat/ plasma fraction (PRP) was resuspended in 20 mL of residual plasma and used in the platelet gel.

2.3 Tissue-engineered bone preparation

The PRP was stored at 22°C in a conventional shaker until used. Human thrombin in a powder form (5000 units) was dissolved in 5 mL of10% calcium chloride in a separate sterile cup. Next, 3.5 mL of PRP, MSCs (1.0×10^7 cell/mL), and air were aspirated into a 5-mL sterile syringe. In a second 2.5 mL syringe, 500 µL of the thrombin/calcium chloride mixture was aspirated. The cells were resuspended directly into the PRP. The 2syringes were connected with a T connector and the plungers of the syringes were alternatively pushed and pulled allowing the air bubble to transverse the 2 syringes. Within 5 to 30 seconds, the contents assumed a gel-like consistency as the thrombin affected the polymerization of the fibrin to produce an insoluble gel(Fig. 1a, b).

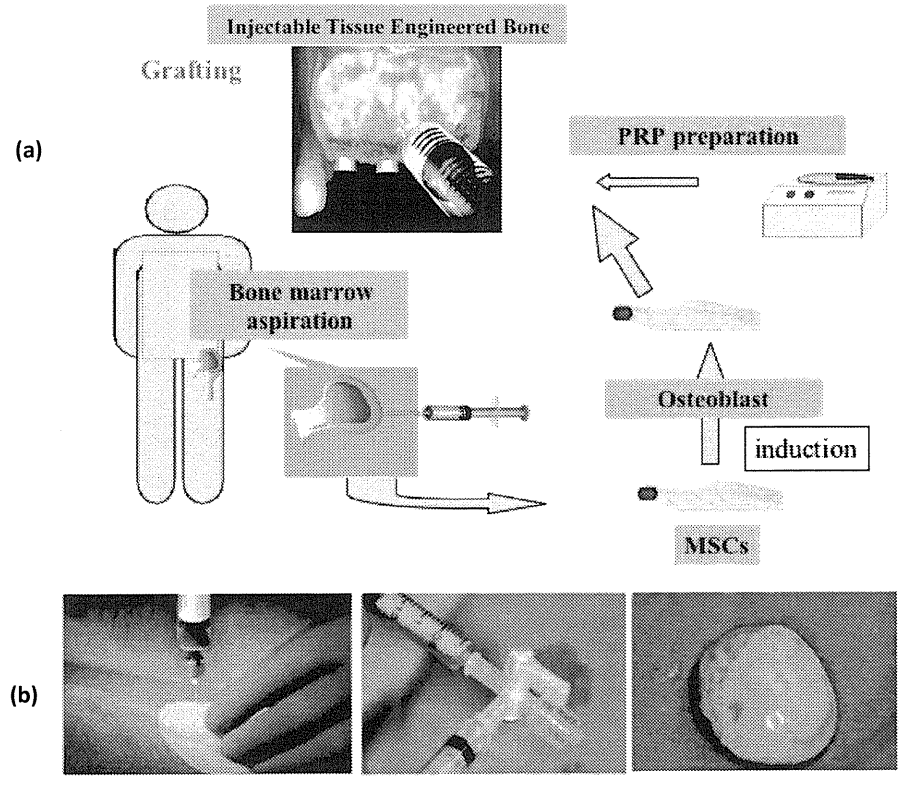

Fig. 1 (a) Outline of preparation of tissue-engineered bone (T.E.B.). (b) Tissue-engineered bone (T.E.B.). Mesenchymal stem cells (MSCs) were isolated from the patient's iliac crest marrow aspirates (left). The osteoblastic differentiated MSCs were mixed with human thrombin, which was dissolved with 10% calcium chloride, and the patient's platelet rich plasma (PRP) (middle). Prepared T.E.B.(right).

2.4 Cell growth and differentiation

The average cell number at the time of transplantation was 18.2 x 10^6 cells. However, the cell proliferating capability varied among individuals. Similar findings were observed in terms of cell differentiation. Even though the exact same induction protocol was used, the final harvested cell number and the levels of ALP activity varied among individuals.

2.5 Patient selection

There were 22 cases with severely resolved alveolar ridge in maxilla aged from 43 to 64 years (mean age 55.6 years). The patients with partially or totally edentulous ridges in maxilla were scheduled for sinus floor grafting. All patients had conventional denture retention problems because of severe anterior or posterior alveolar ridge atrophy. All cases of the maxilla, patients had a residual sinus floor of less than 5 mm in height, to such an extent that the sinus graft and implant would have resolved the problem.

After routine oral and physical examinations, patients were selected and tissue engineered bone grafting was planned because the patients preferred not to undergo any surgery for harvesting of the autogenous bone. In 19 cases, the sinus floor elevation was performed at the part of the posterior maxilla with simultaneous implant placement. In 3 cases, the sinus floor elevation with tissue engineered bone grafting and secondary implant placement was performed (Table 1).The patients were informed extensively about the procedures, including the surgery, graft material, implants, and uncertainties of using a new bone-regenerative method. They were asked for their cooperation during treatment, and the research protocol was approved by the university ethics committee.

2.6 Exclusion criteria

Patients with diabetes and/or autoimmune diseases, who presented hemorrhagic diathesis where partial thromboplastin time (PT) was lower than 50% and activated partial thromboplastin time (APTT) less than 23.5 or longer than 42.5 seconds, uncontrollable infectious diseases, osteoporosis, liver dysfunction with a Glutamic Oxaloacetic Transaminase (GOT) value less than 10 or more than 40 IU/L or with a glutamic pyruvic transaminase (GPT) less than 5 or more than

Table 1 List of the cases of the sinus floor elevation with T.E.B.

Pt.	Age	Gender	Location	Number of implants	Number of cells(x10^6)	Amount of TEB(ml)	Simaltaneous implant	Bone biopsy
1	50	F	14,15,16	3	10	1.2	Yes	
2	54	F	15,16,17	3	5.4	0.6	Yes	
			25,26,27	3	3.6	0.6	Yes	
3	48	M	15,16,17	3	10	2.1	Yes	
			25,26,27	3	10	2.1	Yes	
4	57	F	15,16,17	3	27.6	3.6	Yes	*
5	58	F	25,26,27	3	10	6.6	Yes	*
6	55	M	14,15,16,17	4	46	3.6	Yes	*
			24,25,26,27	4	44	4.8	Yes	*
7	55	F	13,14,15,16,17	5	36	1.8	Yes	
			24,25,26,27	4	36	1.8	Yes	
8	59	F	15,16,17	3	10	1.8	Yes	
			24,25,26,27	4	10	1.8	Yes	
9	54	F	14,15,16	2	10	4	Yes	
10	62	F	15,16	2	9.7	3.9	Yes	
11	60	F	24,25,26	3	20	3.6	Yes	*
12	43	F	25,26	2	10	3.6	No	*
13	57	F	15,16	2	10	2	Yes	
14	59	F	14,15,16,17	4	10	3.6	No	
15	62	F	26,27	2	12	1.8	No	
16	64	M	25,26,27	3	20	0.5	Yes	
17	56	F	25,26,27	3	unknown	unknown	Yes	
18	51	F	14,15,16,17	3	10	unknown	Yes	
19	55	F	14,15,16,17	4	unknown	unknown	Yes	
			14,15,16,17	4	unknown	unknown	Yes	
20	44	F	15,16	2	64	unknown	Yes	
21	66	F	24,25,26	3	unknown	unknown	Yes	*
22	55	F	15,16,17	3	20	unknown	Yes	

45 IU/L, pregnant or possible pregnancy, allergy to any of the medications used in this study and/or the presence of allergy that required continuous systemic medication and other special conditions that the responsible physician considered not appropriate were excluded.

2.7 Surgical technique

In all 22 patients, surgery was carried out under general anesthesia. The sinus grafting procedure followed Tatum's classical description (Tatum, 1986). In brief, after the elevation of a mucoperio steal flap, a door was created with a round hollow bur in the lateral maxillary sinus wall. After mobilization, the door was reflected inward. The space created by this procedure was filled with 0.5 to 6.6 cc of tissue-engineered bone (mean 2.63cc).Care was taken to keep the inner epithelial lining intact to avoid spilling the grafting material. The mucoperio steal flap was repositioned and sutured in the usual manner (Fig.2). In case of 2-step implant procedure, dental implants were installed six months after transplantation. Totally 87 implants were installed in the grafted area (Table 1).

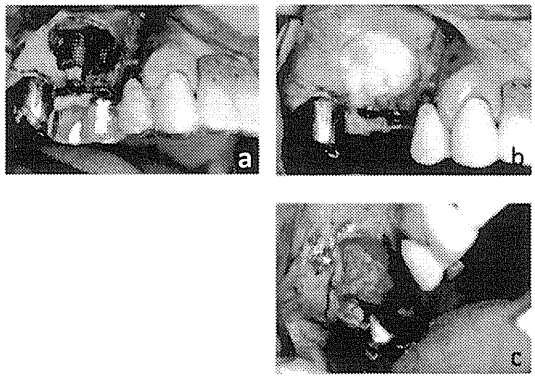

Fig. 2 T.E.B. application for maxillary sinus floor elevation with simultaneous dental implant installation.
(a) Maxillary sinus was elevated with the lateral window technic and the dental implants were installed simultaneously.
(b) The elevated maxillary sinus floor was filled with T.E.B.
(c) Implanted T.E.B. was completely ossificated six months after first surgery.

2.8 Radiographic Analysis

Before and 1, 6, 12 and 24 months after the first surgery, radiographic evaluations using panorama X-ray and CT scan were performed. In panorama X-ray analysis, the bone heights along the installed dental implants were measured. Volume of the regenerated bone were evaluated using Osirix® imaging software (Ver.3.9. http://www.osirix-viewer.com/). We then completed the area of newly regenerated bone (mm^2) among the patients and estimated the area by calculating the mean value.

2.9 Histomorphometric Analysis

A bone biopsy was performed in 5 cases at 6 months after cell transplantation at the time of dental implant installation using a trephine bur (2 mm inner diameter and 3 mm outer diameter; Stoma am Mark GmbH, Emmingen-Liptingen, Germany). After embedding in resin, non-decalcified ground sections were prepared and the sections evaluated with Villanueva bone staining, Villanueva Goldner staining or Hematoxylin and Eosin (H-E) staining. Light microscope images were captured with a digital camera (Carl Zeiss AG, Oberkochen, Germany) and transferred to a computer. The extent of new bone area, the area of fibrous tissue and the area of bone marrow-like tissue were manually assessed using Image J software (Scion Corporation, Frederick, MD, USA) by an examiner. The size of these specific areas was expressed as a percentage of the total area of the section.

3.0 Results

3.1 Clinical and radiographic observations

In case of sinus floor augmentation, evaluation was done from 2 to 5years after the first surgery. The main complications during surgery were sinus membrane perforation and wound separation. Perforation of the sinus mucosa was recorded in 4 procedures and resulted in only minor postoperative nasal bleeding without severe inflammatory sign in maxillary region during total observation period. None of the patients had postoperative problems besides normal swelling and inflammation at the surgical sites.

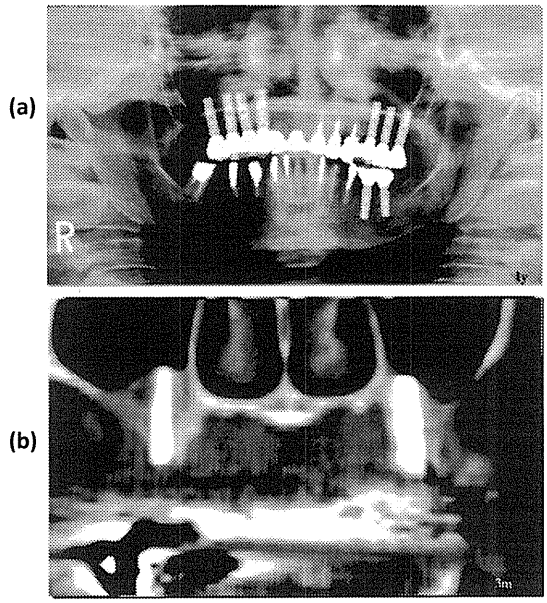

Fig. 3 Radiographic evaluation: a)Panorama X-ray 1 year after the surgery. Mineralized tissue was observed around the dental implants. b)The CT images showed that T.E.B. had already mineralized three months after the surgery.

Pre- and postoperative radiographic evaluations showed that the increasing in mineralized tissue was 8.7 mm in height (Fig.3a, b). Volume of the regenerated bone was analyzed using CT data and software at 6 months, 12 months and 24 months after cell transplantation. Generally, the volume decreased over time though the time course varied among individuals. At the second surgery, which was performed after a mean healing period of 4.8 months, the mucosal flap was elevated to observe the grafted site. In all cases of sinus floor augmentation surgery the spaces around the titanium fixtures were filled with newly formed tissue, which seemed to be calcified tissue.

Eighty-seven fixtures were installed with tissue-engineered bone. Cumulative survival and success rates for fixtures placed in conjunction tissue engineered bone were 100%.Postoperative radiographic findings around the fixtures were consistent with integration between the implant and the regenerated bone (no bone loss or peri-implant radio lucency).At 6 months after loading, as tested after removal of the prosthetic reconstruction, all implants maintained stability.

Marginal bone resorption at 6 months after loading did not exceed 1.5 mm.

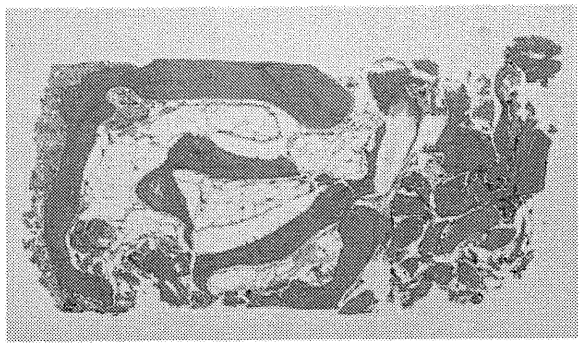

Fig. 4 Histrogical evaluation: A bone biopsy was performed in some cases. Newly regenerated bone was seen without any severe infiltration of inflammatory cells (H-E, x40).

3.2 Histomorphometric Analysis

Although there was variation in new bone area among individuals, the average bone area was 41.9% at 6 months after cell transplantation (Fig.4). This was a major component of the regenerated bone in some of the samples and generally inversely related to the amount of new bone formation. The correlation between transplanted cell numbers, amount of the tissue-engineered bone, transplanted cell density and new bone was shown in Fig 5a,b and c. From these analyses, there were no correlation between these parameters and new bone.

Table 2 Summary of the T.E.B. application for sinus floor elevation

Sinus floor elevation with Tissue Engineered Bone	
・Cases	:22
・Site	:28
・Sex	:M:F=3:19
・Cell Number	:3.6x10^6~46x10^6 (average; 18.9x10^6)
・T.E.B.	:0.5~6.6ml (average; 2.63cc)

4.0 Discussion

4.1 Usability of tissue engineered bone

Reconstruction of maxillofacial defects secondary to tumors and trauma relies on different sources of bone grafts with inherent morbidity. Stem cell based tissue engineering is a promising alternative for bone regeneration (Petite *et al.*, 2000; Bianco *et al.*, 2001; Rose *et al.*, 2002). The bone engineering is a fast-moving field with considerable potential clinical applications (Mao *et al.*, 2006; Kaigler *et al.*, 2006; Zhao *et al.*, 2007). Unfortunately, only very small literatures of the above clinical studies except our study make it to the bedside in the form of clinical trials or therapies. Because of practical and ethical reasons, it is sometimes impossible to have proper control groups and therein lays the difficulty of data interpretation.

The aim of this article is to summarize our current research on bone tissue engineering in Nagoya University Hospital and highlight an important translational study that has already been carried out on human subjects. Our studies are small, observational phase 1-type studies with no control groups and they have short-term follows. Despite this, they do provide valuable information and we know that the clinical use of autologous bone marrow derived MSC is relatively safe and does not preclude the use of other techniques in the event of failure.

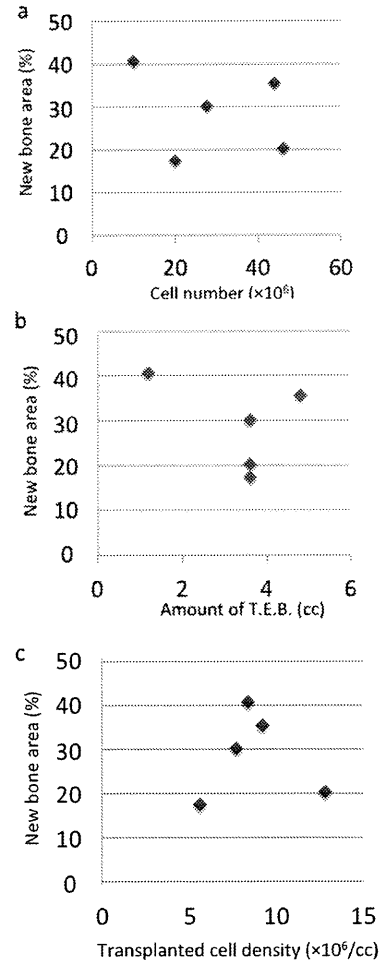

Fig. 5 The correlation between the transplanted cell and the new bone formation. The correlation between the transplanted cell numbers (a), amount of T.E.B. (b), the transplanted cell density (c) and the new bone formation were evaluated. These data indicated that there were no correlation between these three parameters and the new bone formation.